

Electronic Supplementary Information for

**A Porphyrin Covalent Organic Framework Cathode for  
Flexible Zn–Air Batteries**

*Bo-Quan Li, Shu-Yuan Zhang, Bin Wang, Zi-Jing Xia, Cheng Tang, and Qiang Zhang*

Beijing Key Laboratory of Green Chemical Reaction Engineering and Technology,  
Department of Chemical Engineering, Tsinghua University, Beijing 100084, China

Email: [zhang-qiang@mails.tsinghua.edu.cn](mailto:zhang-qiang@mails.tsinghua.edu.cn)

# 1. Experimental Section

## 1.1. Material characterization

The morphology was characterized using a JSM 7401F (JEOL Ltd., Tokyo, Japan) scanning electron microscope (SEM) operated at 3.0 kV and a JEM 2010 (JEOL Ltd., Tokyo, Japan) transmission electron microscope (TEM) operated at 120.0 kV. X-ray Energy-dispersed spectrometer (EDS) and elemental mapping were performed on the JEOL TEM equipped with an Oxford Instrument energy dispersed X-ray spectrometer. Fourier-transform infrared spectrometry (FTIR) was performed on a NEXUS 870 spectrograph to reveal the chemical structure. X-ray diffraction (XRD) patterns were recorded on a Bruker D8 Advanced diffractometer with Cu-K $\alpha$  radiation at 40.0 kV and 120 mA. N<sub>2</sub> adsorption-desorption isotherm was collected using an Auto-IQ2-MP-C system. The Specific surface area (SSA) was calculated based on the multipoint Brunauer–Emmett–Teller (BET) method, and the pore distribution was determined by the quenched solid density function theory (DFT) model using the adsorption branch. X-ray photoelectron spectroscopy (XPS) measurements were carried out by Escalab 250xi with all samples cleaned by argon plasma in advance. All XPS spectra were calibrated using C 1s line at 284.6 eV. Elemental analysis of cobalt content was conducted on a IRIS Intrepid II inductively coupled plasma (ICP) optical emission spectrometer (ThermoFisher, MA, USA). The contact angle analysis was performed on an OCAH200 optical contact angle measuring instrument (Dataphysics, Germany).

## 1.2. Raw materials

Carbon nanotube (CNT) was fabricated according to an improved floating catalyst method, which was reported in our previous work.<sup>[1]</sup> The as-synthesized CNTs are highly aggregated and need further dispersion before serving as templates. Typically, the as-synthesized CNTs were first sheared by a high-speed motor (FLUKO, Batch High Shear FA25, 28000 rpm) in ethanol for 20 min, and the CNT/ethanol suspension was sonicated for another

30 min. After that, the suspension was dried at 60°C for 24 h to afford CNTs suitable as templates for POF hybridization. Reagents including benzene-1,4-dialdehyde (BDA), pyrrole, trifluoroacetic acid (TFA), nitrobenzene (NBZ),  $\text{Co}(\text{CH}_3\text{COO})_2 \cdot 4\text{H}_2\text{O}$ , Pt/C (20 wt.% in Pt), and Ir/C (20 wt.% in Ir) were all purchased from Alfa Aesar and used with no further purification.

### *1.3. Synthesis of CNT@POF*

Porphyrin organic framework (POF) was uniformly coated onto the CNT substrates following an acid-catalyzed dehydration reaction. Specifically, 50.0 mg CNTs were first dispersed in 100 mL acetic acid under ultrasonic treatment for 30 min to form a homogenous suspension. After that, 50.0  $\mu\text{L}$  TFA was added to the suspension as acid catalyst. Subsequently, 9.1  $\mu\text{L}$  pyrrole, 0.45 mL NBZ, 8.7 mg BDA, and 24.9 mg  $\text{Co}(\text{CH}_3\text{COO})_2 \cdot 4\text{H}_2\text{O}$  were mixed with the suspension and sonicated for another 30 min. The as-obtained mixture was kept at 80°C under continuous magnetic stirring for 24 h. The product was filtrated, and washed with deionized water and ethanol for three times to obtain the filter cake. After drying at 60°C overnight, a free-standing, flexible CNT@POF membrane was obtained. Pure POF spheres were synthesized using otherwise identical methods as CNT@POF only without CNT templates.

### *1.4. Rechargeable liquid Zn–air battery assembly*

Rechargeable liquid Zn–air battery performance was evaluated using laboratory-constructed stack-type cells. A polished zinc foil (0.25 mm thickness) and a catalyst-loaded gas diffusion layer (GDL) were used as the anode and the cathode, respectively. The GDL is a conductive carbon layer with polytetrafluoroethylene (PTFE) modification to improve its hydrophobicity. The hydrophobic GDL avoids electrolyte flooding and facilitates air diffusion.

6.0 M KOH containing 0.20 M ZnCl<sub>2</sub> was used as the electrolyte to ensure the electrochemical reversibility at the anode. The electrolyte volume is 0.39 mL.

To fabricate a CNT@POF cathode, a free-standing CNT@POF membrane was hot-pressed with a GDL (1.2 × 1.2 cm<sup>2</sup>) at 80°C for 90 s to form a CNT@POF/GDL hybrid, with a POF areal loading of 1.50 mg cm<sup>-2</sup>. After that, 200.0 μL Nafion solution (0.5 wt%) was drop-cast onto the CNT@POF side as the binder.

To fabricate a Pt/C+Ir/C cathode, 2.5 mg Pt/C, 2.5 mg Ir/C, and 50.0 μL Nafion solution (5.0 wt.% in ethanol) were first dispersed in 950.0 μL ethanol, followed by 1.0 h sonication to form a homogenous catalyst ink. Subsequently, a cleaned carbon cloth (CC) substrate (WOS 1002, CeTech) was hot-pressed with a GDL (1.2 × 1.2 cm<sup>2</sup>) at 80°C for 90 s. A certain volume of catalyst ink was transferred onto CC side of the CC/GDL hybrid *via* a controlled drop casting method to obtain a catalyst areal loading of 1.50 mg cm<sup>-2</sup>.

The fabrication of a CNT+POF cathode is otherwise identical to that of the Pt/C+Ir/C cathode except using 5.0 mg POF spheres instead of 2.5 mg Pt/C + 2.5 mg Ir/C to prepare the catalyst ink and using a pure CNT membrane instead of the CC substrate as the catalyst layer. The areal loading of POF spheres on CNT is 1.50 mg cm<sup>-2</sup>.

### *1.5. Flexible all-solid-state Zn–air battery assembly*

A CNT@POF membrane with the size of 0.5 × 2.0 cm<sup>2</sup> was directly used as the cathode, and a polished flexible zinc foil (0.1 mm thickness) served as the anode. The gel polymer electrolyte was prepared as follows: 1.0 g polyvinyl alcohol (PVA) powder (MW ~19500, Aladdin) was dissolved in 10 mL deionized water at 95°C under magnetic stirring for about 2.0 h. Next, 1.0 mL of 18.0 M KOH aqueous solution containing 0.20 M ZnCl<sub>2</sub> was added and the mixture was kept stirring at 95°C for 40 min. After that, the solution was poured onto a glass plate to form a thin electrolyte film. The film was kept in a freezer at -3°C over 12 h, and then thawed at room temperature. The above procedure was repeated twice to guarantee the

robustness of gelation. Then the CNT@POF membrane and the flexible zinc foil were respectively placed on the two sides of PVA gel electrolyte, and a piece of pressed Ni foam was used as current collector outside the air electrolyte.

### 1.6. Zn–air battery test

All Zn–air batteries were tested under ambient atmosphere at 20°C with an electrochemical workstation (CHI 760E, CH Instrument, USA). The polarization curve measurements were carried out by linear sweep voltammetry at a scan rate of 5 mV s<sup>-1</sup> with 95% *iR*-compensation. Power density is calculated based on the discharge curve using the following equation:  $P=U \times j$ , where  $P$  is the power density,  $U$  is the discharge voltage, and  $j$  is the discharge current density. Galvanostatic charge-discharge cycling tests were conducted using a recurrent galvanic pulse method with each cycle being 20 min (10 min discharge followed by 10 min charge). Specific capacities were determined by the galvanostatical discharge results, normalized to the mass of consumed Zn. Considering the discharge/charge current and time being constants, the energy efficiency is calculated using the following equation:

$$\text{Energy efficiency} = \frac{E_{dis}}{E_{cha}} \times 100\% = \frac{U_{dis}}{U_{cha}} \times 100\%$$

where  $E_{dis}/E_{cha}$  are the discharge/charge energy and  $U_{dis}/U_{cha}$  are the discharge/charge voltage.  $U_{dis}/U_{cha}$  can be directly determined according to the galvanostatic discharge-charge cycling curves.

## 2. Supplementary Figures

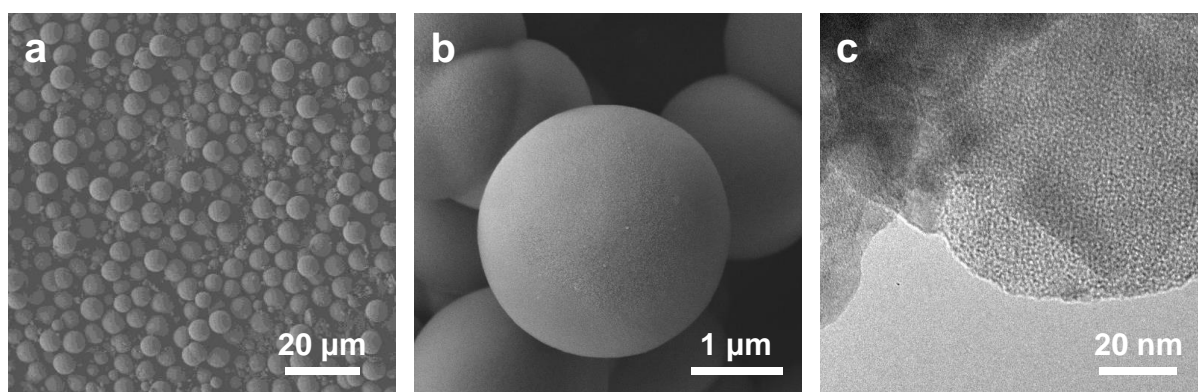


**Fig. S1.** Morphological characterization of pure POF. (a) and (b) SEM images of POF at different magnifications, exhibiting a dense sphere morphology. (c) TEM image at the edge of POF spheres. A typical flake-like morphology was observed at the edge of POF spheres, indicating the intrinsic two-dimensional structure of POF.

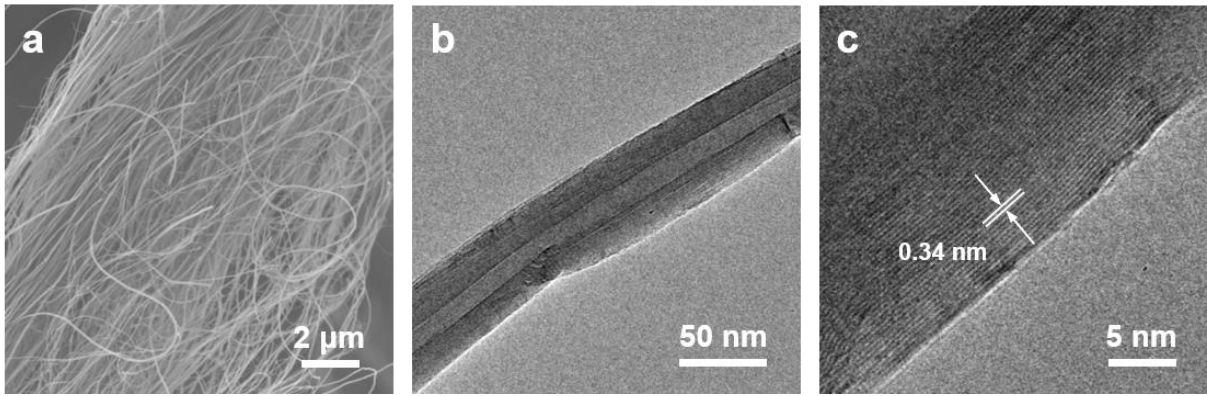


**Fig. S2.** Morphological characterization of CNTs. (a) SEM, (b) TEM and (c) high-resolution TEM images of CNTs.

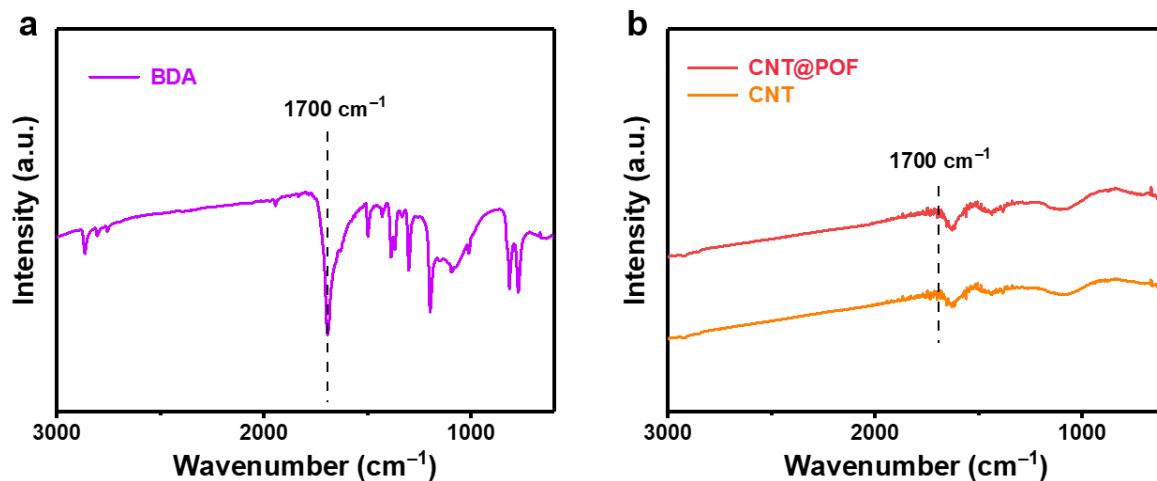


**Fig. S3.** FTIR spectra of POF precursors, CNT, and CNT@POF. (a) FTIR spectrum of BDA. The evident adsorption peak at  $1700\text{ cm}^{-1}$  is assigned to the C=O vibration of BDA. (b) FTIR spectra of CNT and CNT@POF. Compared with pure CNT, CNT@POF exhibits no adsorption peak at  $1700\text{ cm}^{-1}$ , demonstrating the conversion of precursors to POF.

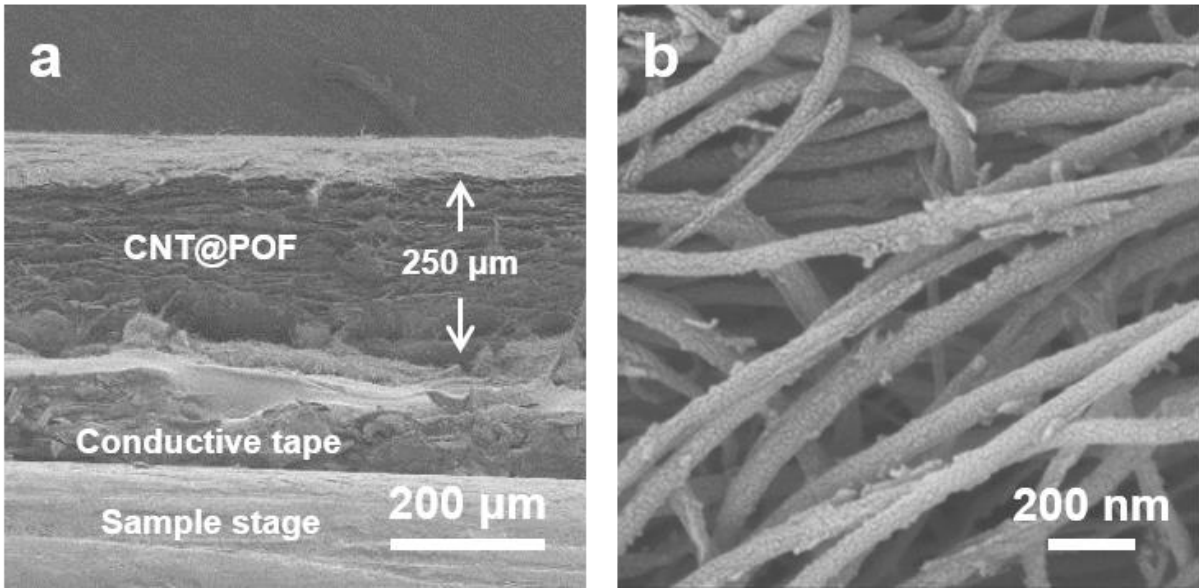


**Fig. S4.** Morphological characterization of the CNT@POF membrane. SEM images of the CNT@POF membrane from (a) the side view and (b) the top view.

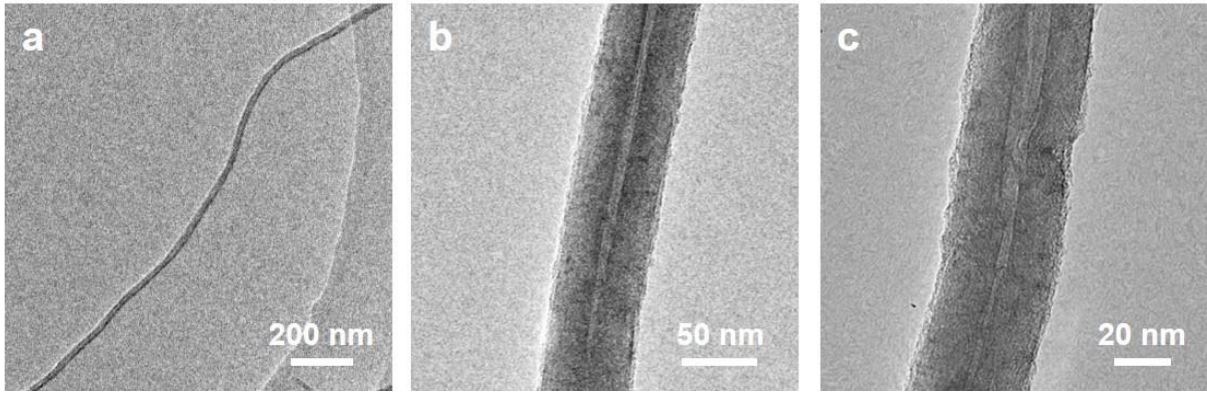


**Fig. S5.** TEM images of CNT@POF.

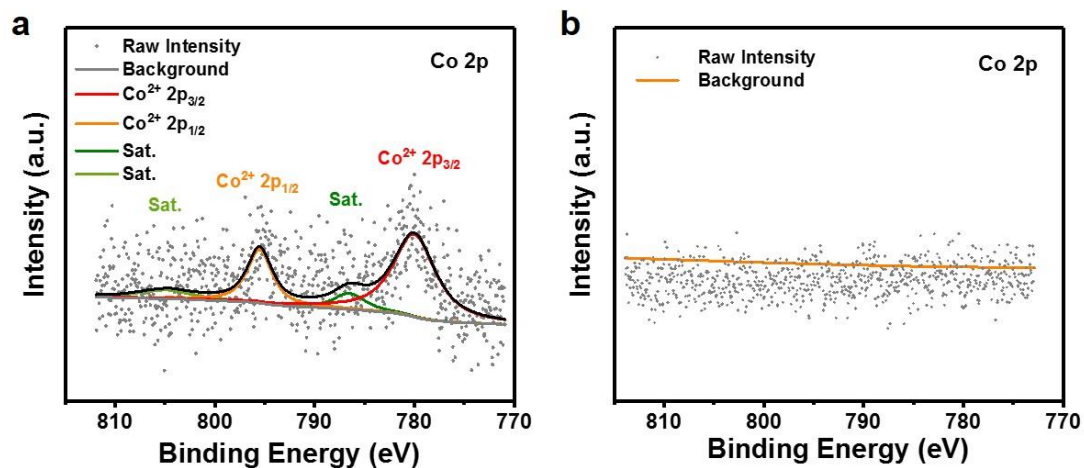


**Fig. S6.** High-resolution Co 2p XPS spectrum of (a) CNT@POF and (b) CNT. Besides Co<sup>2+</sup> 2p<sub>3/2</sub> and Co<sup>2+</sup> 2p<sub>1/2</sub> peaks, two satellite peaks are detected in CNT@POF, demonstrating the +2 oxidation state of cobalt coordinated within POF. By contrast, no cobalt signal was observed and therefore deconvolution cannot be applied.

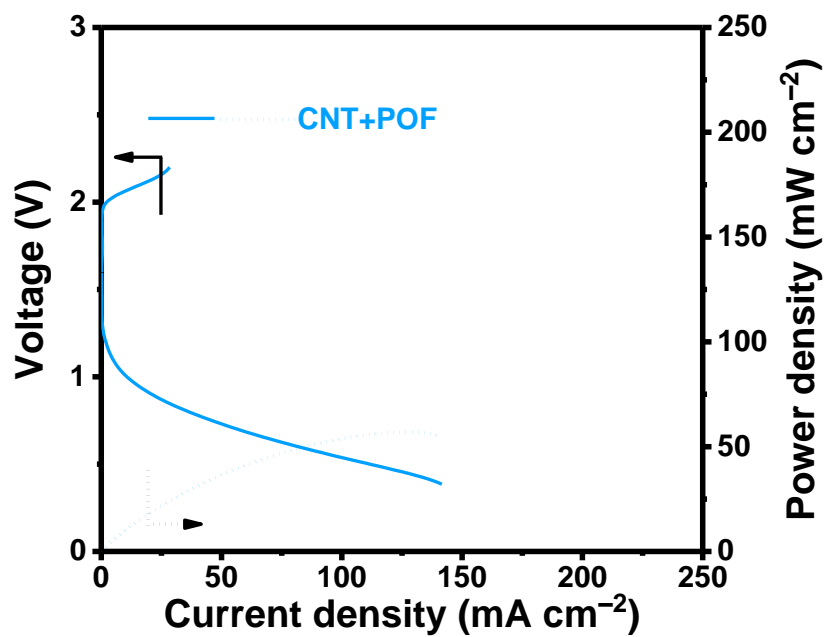


**Fig. S7.** Polarization curves of the CNT+POF cathode and power density calculated according to the discharge branch .

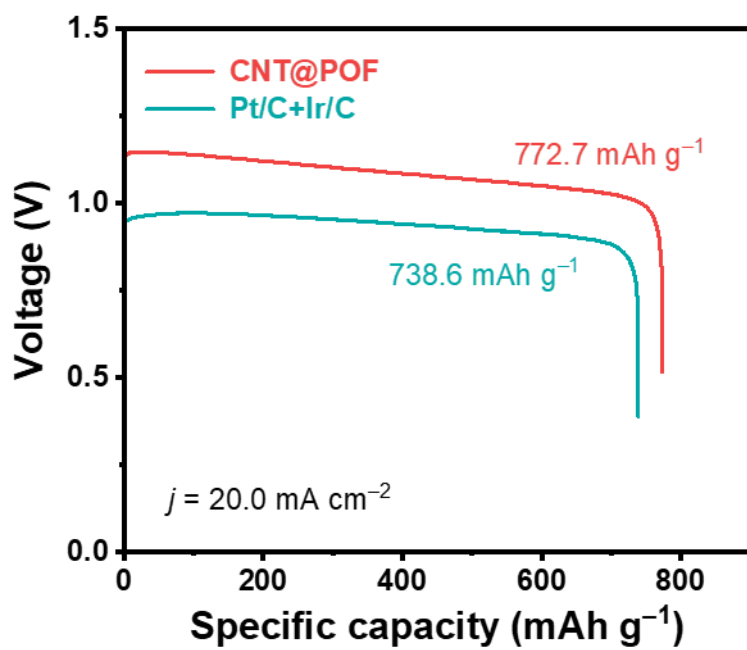


**Fig. S8.** Galvanostatical discharge curves of liquid Zn–air batteries assembled with Pt/C+Ir/C or CNT@POF cathodes at  $20.0 \text{ mA cm}^{-2}$ . The Pt/C+Ir/C cathode and the CNT@POF cathode achieve specific capacities of  $738.6$  and  $772.7 \text{ mAh g}^{-1}$ , respectively.

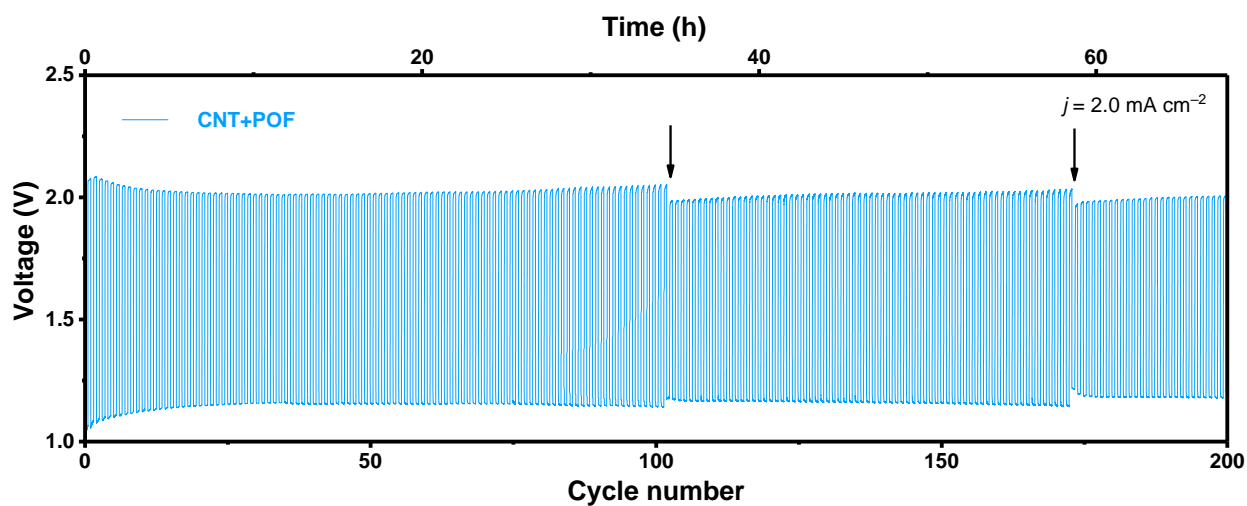


**Fig. S9.** Long time discharge-charge cycling curve of liquid Zn-air battery with the CNT+POF cathode at the current density of  $2.0 \text{ mA cm}^{-2}$ . The electrolyte was replaced as the arrow noted.

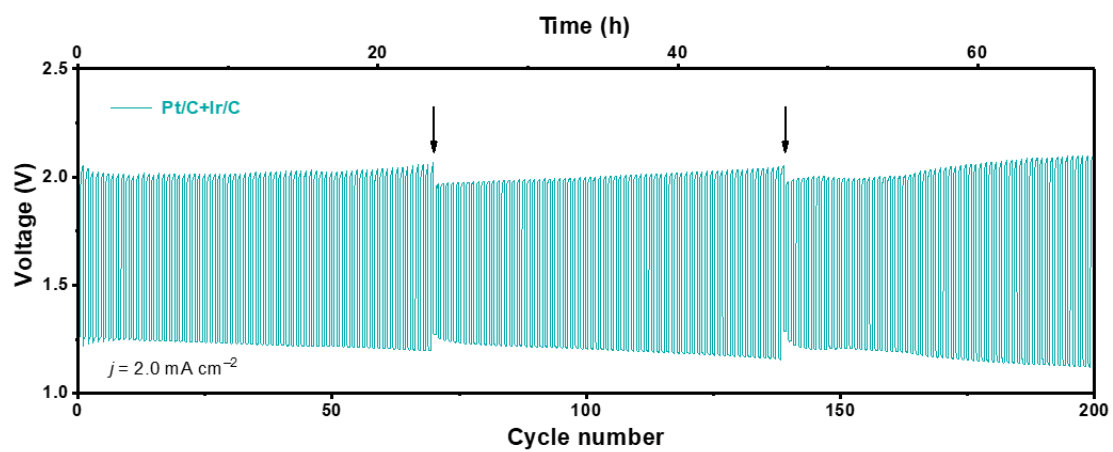


**Fig. S10.** Long time discharge-charge cycling curve of liquid Zn-air battery with the Pt/C+Ir/C cathode at the current density of  $2.0 \text{ mA cm}^{-2}$ . The electrolyte was replaced as the arrow noted.

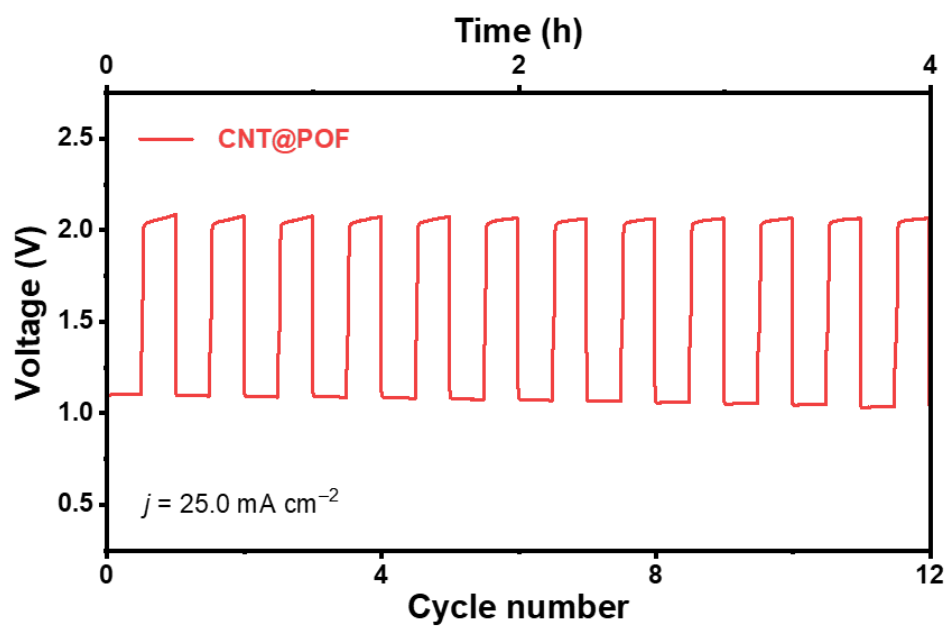


**Fig. S11.** Cycling curve of liquid Zn–air battery with the CNT@POF cathode at a current density of  $25.0 \text{ mA cm}^{-2}$ .

### 3. Supplementary Tables

**Table S1.** Summary of composition of CNT and CNT@POF.

Sample	Method	Relative amounts of elements			
		C	N	O	Co
CNT@POF	XPS (at.%)	83.9	6.5	9.2	0.38
	ICP ( $\mu\text{g g}^{-1}$ )	/	/	/	388.6
CNT	XPS (at.%)	98.5	0.30	1.2	0.0
	ICP ( $\mu\text{g g}^{-1}$ )	/	/	/	Not Detected

**Table S2.** The performance of rechargeable liquid Zn–air batteries with various electrocatalysts. The corresponding current density ( $\text{mA cm}^{-2}$ ) for charge/discharge voltage gap is listed in this Table (after @ in each cell).

Catalyst	Loading amount ( $\text{mg cm}^{-2}$ )	Electrolyte	charge/discharge voltage gap (V)	Peak power density ( $\text{mW cm}^{-2}$ )	Cycling condition ( $\text{mA cm}^{-2}$ )	Stability	Reference
CNT@POF			0.71@2	237		20 min/cycle for 200 cycles, negligible voltage change	
CNT+POF	1.5	6.0 M KOH + 0.20 M $\text{ZnCl}_2$	0.83@2	57	2	20 min/cycle for 200 cycles, voltage gap increased $\sim 0.1$ V	this work
Pt/C+Ir/C			0.81@2	78		20 min/cycle for 200 cycles, voltage gap increased $\sim 0.2$ V	
NMPC-1000	0.5	6.0 M KOH	1.75@2	55	2	10 min/cycle for 180 cycles, voltage gap increased $\sim 0.8$ V	2
NCNF	2	6.0 M KOH + 0.20 M $\text{Zn}(\text{Ac})_2$	$\sim 0.73$ @10	185	10	10 min/cycle for 500 cycles, voltage gap increased $\sim 0.13$ V	3
N-GRW	0.5	6.0 M KOH + 0.20 M $\text{ZnCl}_2$	$\sim 0.86$ @2	65	2	60 min/cycle for 160 cycles, voltage gap increased $\sim 0.16$ V	4
2DBN-800	3	6.0 M KOH + 0.20 M $\text{Zn}(\text{Ac})_2$	1.28@20	14.6	20	10 min/cycle for 66 cycles, negligible voltage change	5

N/S-2DPC-60	3	6.0 M KOH	~0.89@20	0.69	20	10 min/cycle for 72 cycles, negligible voltage change	6
BND2	-	6.0 M KOH	1.40V@16	24.8	16	10 min/cycle for 80 cycles, voltage gap increased ~0.22 V	7
P,S-CNS	-	6.0 M KOH	~1.36@2	198	2	10 min/cycle for 200 cycles, negligible voltage change	8
Co <sub>3</sub> O <sub>4</sub> nanowires/stainless steel	1.5	6.0 M KOH	1.16@~18	~40	~18	10 min/cycle for 100 cycles, voltage gap increased ~0.1 V	9
NC-Co <sub>3</sub> O <sub>4</sub> -90	1.2	6.0 M KOH + 0.10 M Zn(Ac) <sub>2</sub>	0.92@10	-	10	20 min/cycle for ~620 cycles, voltage gap increased ~0.1 V	10
C-CoPAN900 mat	~1	6.0 M KOH + 0.20 M Zn(Ac) <sub>2</sub>	0.85@20	125	20	60 min/cycle for 55 cycles, voltage gap increased ~0.09 V	11
Co <sub>3</sub> O <sub>4</sub> /NPGC	0.9	6.0 M KOH	~0.81@5	~60	5	10 min/cycle for 72 cycles, negligible voltage change	12
NCNT/Co <sub>x</sub> Mn <sub>1-x</sub> O	0.53	6.0 M KOH + 0.20 M ZnO	~0.60@7	~80	7	10 min/cycle for 75 cycles, negligible voltage change	13
CCBC-2	0.72	6.0 M KOH	-	~83	-	10 min/cycle for 75 cycles, voltage gap increased 0.11 V	14
NiCo <sub>2</sub> O <sub>4</sub> -CNTs-400	2	6.0 M KOH	0.75@10	320	10	10 min/cycle for 240 cycles, voltage gap increased 0.15 V	15

MnCo <sub>2</sub> O <sub>4</sub> /NMCNA	-	6.0 M KOH + 0.20 M ZnCl <sub>2</sub>	0.55~0.8@10	~45	10	10 min/cycle for 100 cycles, voltage gap increased 0.25 V	16
NCNT/CoO-NiO- NiCo	0.53	6.0 M KOH + 0.20 M ZnO	0.86@20	~130	20	10 min/cycle for 100 cycles, negligible voltage change	17
Co <sub>4</sub> N/CNW/CC	-	6.0 M KOH + 0.20 M ZnCl <sub>2</sub>	0.84@10	174	10	20 min/cycle for 408 cycles, negligible voltage change	18
Co <sub>3</sub> FeS <sub>1.5</sub> (OH) <sub>6</sub>	0.5	6.0 M KOH + 0.20 M ZnCl <sub>2</sub>	0.84@2	113	2	20 min/cycle for 108 cycles, negligible voltage change	19
NiCo <sub>2</sub> S <sub>4</sub> /N-CNT	1.0	6.0 M KOH + 0.20 M ZnCl <sub>2</sub>	0.63@10	147	10	400 s/cycle for ~150 cycles, voltage gap increased 0.06 V	20
NGM-Co	0.5	6.0 M KOH + 0.20 M ZnCl <sub>2</sub>	~1.00@2	152	2	20 min/cycle for 180 cycles, voltage gap increased ~0.12 V	21
N-GCNT/FeCo-3	2	6.0 M KOH + 0.20 M Zn(Ac) <sub>2</sub>	1.49@120	89.3	120	10 min/cycle for 240 cycles, negligible voltage change	22
3D-CNTA	2	6.0 M KOH + 0.20 M Zn(Ac) <sub>2</sub>	0.68@10	157.3	10	10 min/cycle for 240 cycles, voltage gap increased 0.14 V	23

#### 4. Supplementary References

1. Q. Zhang, D.-G. Wang, J.-Q. Huang, W.-P. Zhou, G.-H. Luo, W.-Z. Qian and F. Wei, *Carbon*, 2010, **48**, 2855-2861.
2. J. Zhang, Z. Zhao, Z. Xia and L. Dai, *Nat. Nanotechnol.*, 2015, **10**, 444-452.
3. Q. Liu, Y. Wang, L. Dai and J. Yao, *Adv. Mater.*, 2016, **28**, 3000-3006.
4. Y. Lu, J. B. Goodenough and Y. Kim, *J. Am. Chem. Soc.*, 2011, **133**, 5756-5759.
5. X. Zhuang, D. Gehrig, N. Forler, H. Liang, M. Wagner, M. R. Hansen, F. Laquai, F. Zhang and X. Feng, *Adv. Mater.*, 2015, **27**, 3789-3796.
6. Y. Su, Z. Yao, F. Zhang, H. Wang, Z. Mics, E. Cánovas, M. Bonn, X. Zhuang and X. Feng, *Adv. Funct. Mater.*, 2016, **26**, 5893-5902.
7. Y. Liu, S. Chen, X. Quan, H. Yu, H. Zhao, Y. Zhang and G. Chen, *J. Phys. Chem. C*, 2013, **117**, 14992-14998.
8. S. S. Shinde, C. H. Lee, A. Sami, D. H. Kim, S. U. Lee and J. H. Lee, *ACS Nano*, 2017, **11**, 347-357.
9. D. U. Lee, J.-Y. Choi, K. Feng, H. W. Park and Z. Chen, *Adv. Energy Mater.*, 2014, **4**, 1301389.
10. C. Guan, A. Sumboja, H. Wu, W. Ren, X. Liu, H. Zhang, Z. Liu, C. Cheng, S. J. Pennycook and J. Wang, *Adv. Mater.*, 2017, **29**, 1704117.
11. B. Li, X. Ge, F. W. Goh, T. S. Hor, D. Geng, G. Du, Z. Liu, J. Zhang, X. Liu and Y. Zong, *Nanoscale*, 2015, **7**, 1830-1838.
12. B. Nath, W.-H. Li, J.-H. Huang, G.-E. Wang, Z.-h. Fu, M.-S. Yao and G. Xu, *CrystEngComm*, 2016, **18**, 4259-4263.
13. X. Liu, M. Park, M. G. Kim, S. Gupta, X. Wang, G. Wu and J. Cho, *Nano Energy*, 2016, **20**, 315-325.
14. Z. Chen, A. Yu, D. Higgins, H. Li, H. Wang and Z. Chen, *Nano Lett.*, 2012, **12**, 1946-1952.

15. C. Ma, N. Xu, J. Qiao, S. Jian and J. Zhang, *Int. J. Hydrogen Energy*, 2016, **41**, 9211-9218.
16. D. Bin, Z. Guo, A. G. Tamirat, Y. Ma, Y. Wang and Y. Xia, *Nanoscale*, 2017, **9**, 11148-11157.
17. X. Liu, M. Park, M. G. Kim, S. Gupta, G. Wu and J. Cho, *Angew. Chem. Int. Ed.*, 2015, **54**, 9654-9658.
18. F. Meng, H. Zhong, D. Bao, J. Yan and X. Zhang, *J. Am. Chem. Soc.*, 2016, **138**, 10226-10231.
19. H. F. Wang, C. Tang, B. Wang, B. Q. Li and Q. Zhang, *Adv. Mater.*, 2017, **29**, 1702327.
20. X. Han, X. Wu, C. Zhong, Y. Deng, N. Zhao and W. Hu, *Nano Energy*, 2017, **31**, 541-550.
21. C. Tang, B. Wang, H. F. Wang and Q. Zhang, *Adv. Mater.*, 2017, **29**, 1703185.
22. C.-Y. Su, H. Cheng, W. Li, Z.-Q. Liu, N. Li, Z. Hou, F.-Q. Bai, H.-X. Zhang and T.-Y. Ma, *Adv. Energy Mater.*, 2017, **7**, 1602420.
23. S. Wang, J. Qin, T. Meng and M. Cao, *Nano Energy*, 2017, **39**, 626-638.